J|A|C|S
ARTICLES
Published on Web 09/14/2004

Strong Exchange Interactions between Two Radicals Attached to Nonaromatic Spacers Deduced from Magnetic, EPR, NMR, and Electron Density Measurements

Raymond Ziessel*,† Christophe Stroh,† Henrike Heise,‡,⊥ Frank H. Köhler,‡ Philippe Turek,§ Nicolas Claiser,|| Mohamed Souhassou,|| and Claude Lecomte||

Contribution from the Laboratoire de Chimie Moléculaire, Ecole de Chimie, Polymères et Matériaux (ECPM), UMR 7008, Université Louis Pasteur (ULP), 25, rue Becquerel, F-67087 Strasbourg Cedex 2, France; Department Chemie, Technische Universität München, D-85747 Garching, Germany; Institut Charles Sadron, Université Louis Pasteur (ULP), 6, rue Boussingault, F-67083 Strasbourg Cedex, France; and LCM3B, CNRS UMR 7036, Faculté des Sciences, Université Henri Poincaré Nancy I, BP 239, F-54506 Vandoeuvre-lès-Nancy, France

Received October 23, 2003; Revised Manuscript Received March 24, 2004; E-mail: ziessel@chimie.u-strasbg.fr

Abstract: A nitronyl-nitroxide (NIT) biradical **D-NIT2** linked by a single double bond has been engineered and investigated in the solid state by a combination of X-ray diffraction, magnetic susceptibility measurement, EPR, as well as solid-state ^{1}H and ^{13}C NMR spectroscopies, and experimental electron density distribution. All techniques reveal that a double bond is a very efficient coupling unit for exchange interactions between two radical moieties. Using a Bleaney−Bowers model dimer ($H = -J\mathbf{S_1}\mathbf{S_2}$), a singlet−triplet energy gap of $J = -460$ K was found with the singlet state being the ground state. This very strong intramolecular interaction was confirmed by EPR measurements in CH_2Cl_2 solution (6 10^{-4} M) or dispersed in a polymer matrix at low concentration. In keeping with these unusual interactions, solid-state NMR signals of the biradical were found to be considerably less shifted than those found for related monoradicals. Temperature-dependent solid-state ^{13}C NMR spectra of **D-NIT2** confirmed the very strong intramolecular coupling constant ($J = -504$ K). The electron density distribution of **D-NIT2** was measured by high resolution X-ray diffraction, which also revealed that this biradical is an ideally conjugated system. The in-depth characterization includes the deformation maps and the observed electron density ellipticities, which exhibit a pronounced $\sigma-\pi$ character of the O−N−C=C−N−O cores in keeping with an efficient electronic delocalization along the alkene spacer.

Introduction

The search for new molecular materials with relevant magnetic properties is a thriving subject, experiencing rapid development.[1] Among the various approaches, pure organic radicals play an important role as basic units. Here, seminal discoveries are the β-crystal phase of *p*-nitrophenyl nitronyl-nitroxide[2] and diazaadamantane dinitroxide,[3] both of which undergo transition to the ferromagnetic state at cryogenic temperatures. However, since then the design of stable free radicals has most often led to exchange couplings, which are small and antiferromagnetic in the solid state.[4] The search for strong intermolecular interactions is, therefore, a prerequisite for a magnetic ordering of the spins.[1,5,6] Usually, the magnitude of the intermolecular interactions depends on the distance between the spins, their relative orientation with the exchange

† Laboratoire de Chimie Moléculaire, Ecole de Chimie, Polymères et Matériaux, Université Louis Pasteur (ULP).
‡ Technische Universität München.
§ Institut Charles Sadron, Université Louis Pasteur (ULP).
|| Université Henri Poincaré Nancy I.
⊥ New address: Max-Planck-Institut für Biophysikalische Chemie, Am Fassberg 11, D-37077 Göttingen, Germany.

(1) The literature on this topic is too large to be exhaustively quoted. For some representative books and review articles; see (a) Kahn, O. *Molecular Magnetism*; VCH: New York, 1993. (b) *Molecular Magnetism: From Molecular Assemblies to the Devices*; Coronado, E., Delhaès, P., Gatteschi, D., Miller, J. S., Eds.; Nato ASI Series E, Applied Sciences, Kluwer Academic Publisher: Dordrecht, Netherland, 1996; Vol. 321. (c) *Molecular Magnetism*; Itoh, K., Kinoshita, M., Eds.; Gordon and Breach Science Publisher: Amsterdam, Netherland, 2000. (d) *Magnetism: Molecules to Materials I: Models and Experiments* and *Magnetism: Molecules to Material II: Molecule-Based Materials and Experiments*; Miller, J. S., Drillon, M., Eds.; Wiley-VCH: New York, USA, 2001. (e) *Molecular Magnets: Recent Highlights*; Linert, W., Verdaguer, M., Eds.; Springer-Verlag: Wien, Austria, 2003.

(2) Kinoshita, M.; Turek, P.; Tamura, M.; Nozawa, K.; Shiomi, D.; Nakazawa, Y.; Ishikawa, M.; Takahashi, M.; Awaga, K.; Inabe, T.; Maruyama, Y. *Chem. Lett.* **1991**, 1225.

(3) Chiarelli, R.; Novak, M. A.; Rassat, A.; Tholence, J.-L. *Nature* **1993**, *363*, 147.

(4) (a) Rajca, A. *Chem. Rev.* **1994**, *94*, 871. (b) Lahti, P. M., Ed. *Magnetic Properties of Organic Materials*; Marcel Dekker: New York, 1999. Itoh, K.; Kinoshita, M., Eds. *Molecular Magnetism*; Kodasha: Tokyo and Gordon and Breach Science Publishers: Australia, 2000.

(5) (a) VIIth International Conference on Molecular-based Magnets (ICMM 2000), San Antonio, USA, 16−21 September 2000: *Polyhedron* **2001**, *20*, 1305. (b) Coronado, E., Delhaès, P., Gatteschi, D., Miller, J. S., Eds. *Molecular Magnetism: From Molecular Assemblies to the Devices*; NATO ASI Series E 321; Kluwer Academic Publishers: Dordrecht, 1996.

(6) (a) Romero, F. M.; Ziessel, R.; De Cian, A.; Fischer J.; Turek, P. *New. J. Chem.* **1996**, *20*, 919. (b) Pontillon, Y.; Ressouche, E.; Romero, F. M.; Schweizer J.; Ziessel, R. *Physica B* **1997**, *234*−*236*, 788. (c) Hernàndez, E.; Mas, M.; Molins, C.; Rovira, C.; Veciana, J. *Angew. Chem., Int. Ed. Engl.* **1993**, *32*, 882. (d) Tsugawara, T.; Matsushita, M. M.; Izuoka, A.; Wada, N.; Takeda, N.; Ishikawa, M. *Chem. Commun*. **1994**, 1723.

10.1021/ja0305959 CCC: $27.50

interactions between spins becoming stronger as the distance of the radical centers decreases.[7] Different approaches for shortening the distance between adjacent molecules have been used such as hydrogen bonded networks and Coulombic attractive forces in ionic salts.[8] In general, they show much stronger exchange interaction than van der Waals attraction between neutral organic moieties. Although the strengthened intermolecular coupling among neighboring free radicals is often antiferromagnetic rather than ferromagnetic, the critical ordering temperatures of the unpaired electron spins have been significantly increased during the past decade.[9] Nevertheless, the improvement of the exchange interactions between the spins is necessary to reach room-temperature devices and to develop technological applications.

In recent years, high-spin clusters have attracted much attention in the fields of molecule-based magnetism and solid-state physics in particular due to the emergence of single-molecule magnets (SMMs).[10−13] Beautiful examples have been provided with peculiar magnetic properties such as metastable magnetization,[11] quantum spin tunneling,[12] and quantum phase interference.[13] The fine control of magnetic interaction between adjacent centers is the major target of the development of novel SMMs and giant-spin paramagnetic clusters.[14] Furthermore, the construction of high-spin molecules based on linear, two-dimensional, and starburst polycarbenes[15] has been achieved, and these scaffoldings exhibit very high-spin ground states. Interestingly, these carbon-centered radicals exhibit very strong antiferromagnetic couplings but suffer from low chemical stability. More sterically encumbered triarylmethane radicals are prone to higher chemical stability, and their functionalization seems promising.[16] On the way to stable radicals exhibiting effective ferromagnetic interactions galvinoxyl,[17] verdazyl,[18] dithiadiazolyl,[19] various polyhalogenated polyradicals,[20] and mixed radicals bearing *tert*-butyl nitroxide and nitronyl nitroxide moieties[21] have also been studied. Furthermore, π-conjugated polynitroxides have been employed as bridging ligands, in which the spins of the unpaired electrons interact ferromagnetically.[22] For 1,3-nitroxide-[23] and 1,3,5-nitroxide-substituted[24] benzenes as well as for bent diphenyl grafted triradicals,[25] the magnitude of the exchange coupling between the nitroxide radicals was studied by means of the temperature dependence of their effective magnetic moments. The energy gaps of the high-spin ground state and the low-spin excited states (singlets for biradicals and doubly degenerate doublets for triradicals) cover a range of $+300$ to $+5$ K depending on the topology, flexibility, and conjugation length.[15] The assembly of these high-spin polynitroxide radicals in macroscopic loops and the ordering of their unpaired electrons have been effectively achieved by means of coordination with paramagnetic metal centers.[26] The resulting heterospin systems are of great promise for the rational and versatile design of molecule-based magnets featuring a high Curie temperature, T_c. It is now clear that there are two major factors contributing to a high T_c of such materials: (i) the higher dimensionality of the magnetic structure of the complexes and (ii) the strong exchange coupling within the polynitroxide ligand molecules and across their bonds to metal ions. Recently, a novel 5,10-diphenyl-5,10-dihydrophenazine radical cation substituted by a nitronyl-nitroxide was found to be a stable triplet species with very strong intramolecular ferromagnetic coupling.[27]

As a matter of fact, nonaromatic but unsaturated spacers have rarely been combined with delocalized radicals. In a few cases, double or triple bonds have been used to separate the radical from aromatic groups leading to only weak exchange interactions due to the sterically induced distortion of the conjugated system.[28] Despite this major drawback, these radicals have been used to prepare π-toporegular spin-labeled polymers, some of which displayed very interesting cooperative properties.[29] In our previous studies on the use of alkyne-substituted nitroxide radicals, we found evidence for transmission of ferromagnetic interactions through hydrogen bonds.[30] The topological analysis based on accurate electron density modeling pointed out the particular electronic features of the group carrying the unpaired electron. The N−O bond exhibits a small positive value of the Laplacian associated with a large λ_3 curvature (>40 eÅ^{-5}) and

(7) (a) Stroh, C.; Turek, P.; Ziessel, R. *Chem. Commun*. **1998**, 2337. (b) Pardo, E.; Faus, J.; Julve, M.; Lloret, F.; Munoz, M. C.; Cano, J.; Ottenwaelder, X.; Journaux, Y.; Carrasco, R.; Blay, G.; Fernandez, I.; Ruiz-Garcia, R. *J. Am. Chem. Soc*. **2003**, *125*, 10770.
(8) Inoue, K.; Iwamura, H. *Chem. Phys. Lett.* **1993**, *207*, 551.
(9) Iwamura, H.; Inoue, K.; Hayamizu, T. *Pure Appl. Chem*. **1996**, *68*, 243 and references therein.
(10) Caneschi, A.; Gatteschi, D.; Sessoli, R. *J. Am. Chem. Soc.* **1991**, *113*, 5873.
(11) (a) Sessoli, R.; Tsai, H.-L.; Schake, A. R.; Wang, S.; Vincent J. B.; Folting, K.; Gatteschi, D.; Christou, G.; Hendrickson, D. N. *J. Am. Chem. Soc.* **1993**, *115*, 1804. (b) Eppley, H. J.; Tsai, H.-L.; de Vries, N.; Folting, K.; Christou, G.; Hendrickson, D. N. *J. Am. Chem. Soc.* **1995**, *117*, 301. (c) Aubin, S. M. J.; Sun, Z.; Pardi, L.; Krzystek, J.; Folting, K.; Brunel, L.-C.; Rheingold, A. L.; Christou, G.; Hendrickson, D. N. *Inorg. Chem.* **1999**, *38*, 5329.
(12) (a) Friedman, J. R.; Sarachik, M. P.; Tejada, J.; Ziolo, R. *Phys. Rev. Lett.* **1996**, *76*, 3830. (b) Thomas, L.; Lionti, F.; Ballou, R.; Gatteschi, D.; Sessoli, R.; Barbara, B. *Nature* **1996**, *383*, 145.
(13) Wernsdorfer, W.; Sessoli, R. *Science* **1999**, *284*, 133.
(14) (a) Schake, A. R.; Tsai, H.-L.; Webb, R. L.; Folting, K.; Christou, G.; Hendrickson, D. N. *Inorg. Chem.* **1994**, *33*, 6020. (b) Larionova, J.; Gross, M.; Pilkington, M.; Andres, H.; Stoeckli-Evans, H.; Güdel, H. U.; Decurtins, S. *Angew. Chem., Int. Ed.* **2000**, *39*, 1605. (c) Zhong, Z. J.; Seino, H.; Mizobe, Y.; Hidai, M.; Fujishima, A.; Ohkoshi, S.; Hashimoto, H. *J. Am. Chem. Soc*. **2000**, *122*, 2952. (d) Berseth, P. A.; Sokol, J. J.; Shores, M. P.; Heinrich, J. L.; Long, J. R. *J. Am. Chem. Soc.* **2000**, *122*, 9655. (e) Miyasaka, H.; Nezu, T.; Iwahori, F.; Furukawa, S.; Sugimoto, K.; Clérac, R.; Sugiura, K.-I.; Yamashita, M. *Inorg. Chem.* **2003**, *42*, 4501.
(15) Matsuda, K.; Nakamura, N.; Inoue, K.; Koga, N.; Iwamura, H. *Chem.—Eur. J*. **1996**, *2*, 259.
(16) (a) Rajca, A.; Rajca, S.; Wongsriratanakul, J. *J. Am. Chem. Soc*. **1999**, *121*, 6308. (b) Rajca, A.; Utamapanya, S. *J. Org. Chem*. **1992**, *57*, 176. (c) Sedó, J.; Ventosa, N.; Ruiz-Molina, D.; Mas, M.; Molins, E.; Rovira, C.; Veciana, J. *Angew. Chem., Int. Ed.* **1998**, *37*, 330.
(17) (a) Sugano; T. *Polyhedron* **2001**, *20*, 1285. (b) Barclay, T. M.; Hicks, R. G.; Lemaire, M. T.; Thompson, L. K. *Inorg. Chem*. **2001**, *40*, 6521.
(18) Hicks, R. G.; Lemaire, M. T.; Öhrström, L.; Richardson, J. F.; Thompson, L. K.; Xu, Z. *J. Am. Chem. Soc*. **2001**, *123*, 7154.
(19) (a) Banister, A. J.; Bricklebank, N.; Clegg, W.; Elsegood, M. R. J.; Gregory, C. I.; Lavender, I.; Rawson, J. M.; Tanner, B. K. *Chem. Commun.* **1995**, 679. (b) Barclay, T. M.; Cordes, A. W.; George, N. A.; Haddon, R. C.; Itkis, M. E.; Oakley, R. T. *Chem. Commun*. **1999**, 2269.
(20) Veciana, J.; Rovira, C.; Crespo, M. I.; Armet, O.; Domigo, V. M.; Palacio, F. *J. Am. Chem. Soc*. **1991**, *113*, 2552.
(21) Inoue, K.; Iwamura, H. *Angew. Chem., Int. Ed. Engl*. **1995**, *34*, 927.
(22) Iwamura, H.; Koga, N. *Acc. Chem. Res*. **1993**, *26*, 346.
(23) (a) Ishida, T.; Iwamura, H. *J. Am. Chem. Soc*. **1991**, *113*, 4238. (b) Kanno, F.; Inoue, K.; Koga, N.; Iwamura, H. *J. Am. Chem. Soc*. **1993**, *115*, 847. (c) Catala, L.; Le Moigne, J.; Kyritsakas, N.; Rey, P.; Novoa, J. J.; Turek, P. *Chem.—Eur. J*. **2001**, *7*, 2466.
(24) Kanno F.; Inoue, K.; Koga, N.; Iwamura, H. *J. Phys. Chem*. **1993**, *97*, 13267.
(25) Inoue, K.; Iwamura, H. *Adv. Mater*. **1996**, *8*, 73.
(26) (a) Inoue, K.; Iwamura, H. *J. Am. Chem. Soc.* **1994**, *116*, 3173. (b) Kumagai, H.; Inoue, K. *Angew. Chem., Int. Ed.* **1999**, *38*, 1601. (c) Caneschi, A.; Chiesi, P.; David, L.; Ferraro, F.; Gatteschi, D.; Sessoli, R. *Inorg. Chem*. **1993**, *32*, 1445.
(27) Hiraoka, S.; Okamoto, T.; Kozaki, M.; Shiomi, D.; Sato, K.; Takui, T.; Okada, K. *J. Am. Chem. Soc*. **2004**, *126*, 58.
(28) (a) Inoue, K.; Iwamura, H. *Mol. Cryst. Liq. Cryst*. **1993**, *232*, 89. (b) Wautelet, P.; Le Moigne, J.; Videra, V.; Turek, P. *J. Org. Chem*. **2003**, *68*, 8025.
(29) (a) Inoue, K.; Koga, N.; Iwamura, H. *J. Am. Chem. Soc.* **1991**, *113*, 9803. (b) Miura, Y.; Issiki, T.; Ushitani, Y.; Teki, Y.; Itho, K. *J. Mater. Chem*. **1996**, *6*, 1745.
(30) Romero, F. M.; Ziessel, R.; Bonnet, M.; Pontillon, Y.; Ressouche, E.; Schweizer, J.; Delley, B.; Grand A.; Paulsen, C. *J. Am. Chem. Soc*. **2000**, *122*, 1298.

Scheme 1. (A) Compd **1**·H_2SO_4, MeOH/H_2O 1:5, 60 °C, 3 h, (B) $NaIO_4$, H_2O/CH_2Cl_2

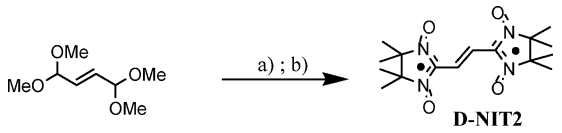

a large electron density at the bond critical point.[31,32] Furthermore, the observed charge delocalization over the whole molecule was linked to the three-dimensional hydrogen bonded network. Interestingly, a bond length alternation in the central spin-containing O−N−C−N−O moiety with short N−O and long C−N bonds was also observed.[32]

In the present work we describe the synthesis of a bis-nitronyl-nitroxide radical that is bridged by one ethylene function. The compound was studied by a single-crystal X-ray analysis and magnetic measurements, as well as by EPR and solid-state MAS NMR spectroscopies, thereby establishing molecular spin density maps. The challenge of preparing a diradical with an unsaturated but nonaromatic spacer was rewarded with very strong intramolecular exchange interactions between the two radical moieties, and all data support the conclusion that unsaturated bonds act as very efficient coupling units.

Results and Discussion.

Synthesis. The synthesis of this diradical (Scheme 1) is challenging and could not be realized by the conventional protocols.[33,34] This is probably due to the low solubility of the bis-carbaldehyde derivatives and to the fact that the first condensation with *N*,*N*′-dihydroxy-2,3-diammonium-2,3-dimethyl-butane **1** deactivates the second aldehyde function to such an extent that formation of the bis-dihydroxyimidazolidine species is inhibited. These difficulties have been bypassed by reacting *N*,*N*′-dihydroxy-2,3-diammonium-2,3-dimethyl-butane sulfate salt, **1**·H_2SO_4, with the protected fumaraldehyde followed by oxidation with $NaIO_4$ in a biphasic mixture. The presence of stoichiometric amounts of acid favors the in situ deprotection of the aldehyde and the condensation steps. The presence of water is required for the solubilization of the hydroxylamine salt.

The product was chemically and photochemically very stable and has been purified by careful chromatography on SiO_2 and by double recrystallization in adequate solvent mixtures. The mass spectra show the intense molecular peak together with fragments characteristic of the successive loss of oxygen atoms, while the N−O stretching frequencies lie at the expected value for nitronyl-nitroxide radicals.

Structural Details of D-NIT2. The diradical contains an inversion center situated in the middle of the double bond of the spacer. The mean planes of both radicals are nearly coplanar with the plane of the olefin, making a dihedral angle of only 1.2° (Figure 1). The nitronyl-nitroxide parts show bond lengths and angles as usually found for such radicals [C1−N1, 1.351(3); C1−N2, 1.353(3); N1−C2, 1.494(3); N2−C3, 1.505(3); C2−C3, 1.553(3); N1−O1, 1.277(2); N2−O2, 1.276(2)]. The distance between the radical junctions C1 and C1′ is 3.79 Å, while the shortest intramolecular distance of the oxygen atoms across the double bond is 4.52 Å.

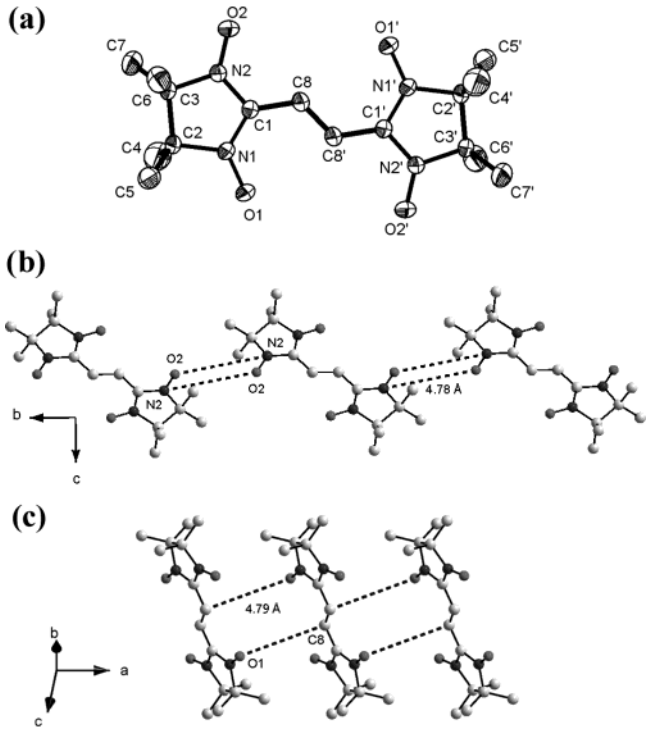

Figure 1. (a) ORTEP view of **D-NIT2** with atom labeling scheme. Displacement ellipsoids are drawn at the 30% probability level, and H atoms are not shown for the sake of clarity: (b) short contacts running along the *b* axis; (c) short contacts running along the *a* axis.

Close examination of the crystal packing shows no intermolecular distance shorter than 4 Å between the ONCNO fragments of the radicals. In fact, the methyl groups of the radical moieties point toward the unsaturated bridge of the neighboring molecule thereby avoiding short contacts between sites with large spin density sites. This is indeed confirmed by the head-to-tail arrangement of neighboring radicals forming a zigzag chain running along the *b* axis (Figure 1b). The shortest distance is 4.78 Å, and the orientation of the magnetic orbitals is not favorable for an efficient overlapping as confirmed by the dihedral angles (O2−N2- - -O2″, $\alpha = 61.0°$ and C1−N2−O2- - -O2″, $\beta = 158.7°$, O2″ belongs to a neighboring molecule as depicted in Figure 1b). Furthermore, some significant contacts exists along the *a* axis between the olefinic carbon atom C8 and the neighboring NO radical (Figure 1c, $d = 4.79$ Å). Here also the orientation of the molecular orbitals is not suitable for an efficient overlapping. Finally, the electron density study of **D-NIT2** at 106 K fully agrees with the room-temperature structure.

Magnetic and EPR Properties. D-NIT2. The value of $\chi T = 0.37$ emu K mol^{-1} at room temperature is very low compared to the expected value for two $S = {}^1/_2$ isolated spins ($\chi T = 0.75$ emu K mol^{-1}) (Figure 2a). Moreover, this curve decreases sharply upon decreasing the temperature, reaching zero at ca. 50 K. The susceptibility-versus-temperature curve is also decreasing with the temperature, dropping to a plateau between 50 and 10 K ($\chi = 2 \times 10^{-5}$ emu mol^{-1}). At very low

(31) Pillet, S.; Souhassou, M.; Pontillon, Y.; Caneschi, A.; Gatteschi, D.; Lecomte, C. *New. J. Chem.* **2001**, *25*, 131.
(32) Claiser, N.; Souhassou, M.; Lecomte, C.; Pontillon, Y.; Romero, F.; Ziessel R. *J. Phys. Chem.* **2002**, *106*, 12896.
(33) (a) Osiecki, J. H.; Ullman, E. F. *J. Am. Chem. Soc*. **1968**, *90*, 1078. (b) Ullman, E. F.; Call, L.; Osiecki, J. H. *J. Org. Chem.* **1970**, *35*, 3623.
(34) Ullman, E. F.; Osiecki, J. H.; Boocock, D. G. B.; Darcy, R. *J. Am. Chem. Soc*. **1972**, *94*, 7049.

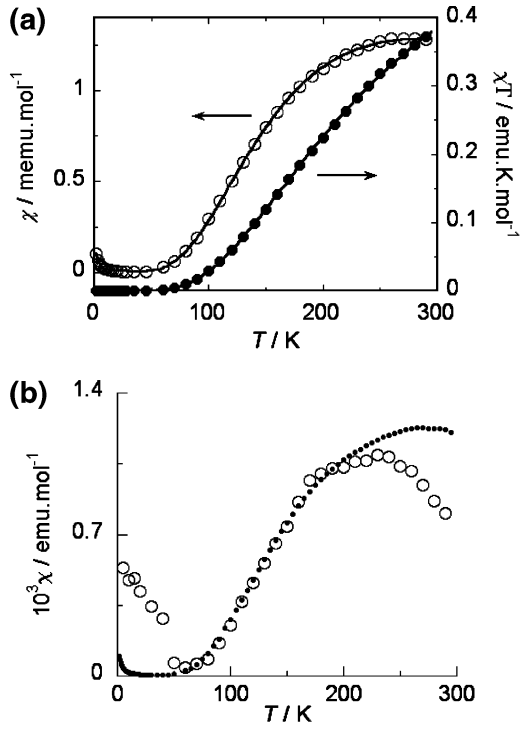

Figure 2. (a) Magnetic susceptibility (χ) and χ·T product versus temperature for a polycrystalline sample of **D-NIT2**, (b) Temperature dependence of the susceptibility measured by SQUID for **D-NIT2** (○ polystyrene matrix, ● polycrystalline sample). The susceptibility of the sample in the polystyrene matrix is scaled such as the low temperature increase up to the maximum susceptibility coincides with the data for the polycrystalline sample.

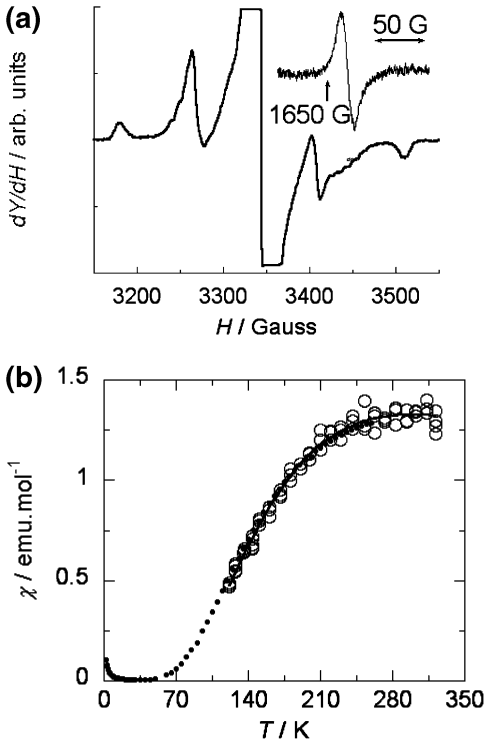

Figure 3. (a) EPR spectra of **D-NIT2** (3%) dispersed in a matrix of polystyrene at room temperature, inset of the $\Delta M_s = \pm 2$ below 128 K, and (b) EPR susceptibility measured for the same sample, the points corresponding to the experimental measurements and the solid line corresponding to the best fit by a Bleaney−Bowers. The dashed line correspond to the susceptibility measured on the polycrystalline sample by SQUID measurements; the inset corresponds to the measured $\Delta M_s = \pm 2$ signal.

temperature, a Curie tail is observed due to a paramagnetic impurity estimated at 0.05% by data fit. In accord with the crystal structure, the magnetic behavior can be modeled with a Bleaney−Bowers model for a dimer of two $S = {}^1/_2$ spins ($H = -J\mathbf{S_1}\mathbf{S_2}$).[35] The best fit ($R = 0.999\,96$) is obtained for the χT curve with a singlet ground state: $\Delta E_{ST} = 460$ K; Curie constant = 0.735 emu K mol^{-1}; including a 0.05% $S = {}^1/_2$ impurity (Curie tail).

SQUID has also measured the susceptibility of the same polystyrene dispersed matrix. Due to the strong diamagnetic contribution, the results remain qualitative but show a curve shape similar to that of the polycrystalline material (Figure 2b).

In diluted CH_2Cl_2 fluid solution (6×10^{-4} M) at room temperature, the EPR spectrum consists of a broad featureless signal centered at $g = 2.0067$ (see Supporting Information Figure S1). The spectral features of nitronyl-nitroxide biradicals in fluid solution depend on the ratio between the magnetic exchange interaction (J) and the hyperfine interaction (a).[34,36] The limit of strong exchange coupling ($|J| \gg |a|$) is obtained for very weak exchange coupling as low as a few tens mK, since a is of the order of a few Gauss. It results in a nine line hyperfine patterns akin to the four equivalent ^{14}N nuclei with the intensity ratio: 1:4:10:16:19:16:10:4:1, with separation $a_N/4$, where a_N equals ca. 15 G for one ^{14}N nucleus. At intermediate exchange ($J \approx a$), the hyperfine pattern exhibits additional lines, which intensity and position strongly depend on $|J|/|a|$. Finally, in the limit of null exchange interaction, i.e., decoupled radicals, the hyperfine structure is the same as that observed for the single radical, i.e., five lines with the intensity ratio: 1:2:3:2:1, with separation $a_N/2$. In the present case, it is worth noting that higher dilutions in different solvents did not alter significantly the signal shape. Since aggregation phenomena were not observed, e.g., by optical UV−vis measurements at similar dilution, intermolecular exchange and/or dipolar interactions could be excluded. The line shape in fluid solution is attributed to (i) a broad Gaussian feature due to direct through-space intramolecular dipolar interactions ($d_{NO-NO} \cong 3.8$ Å) and (ii) the superimposed but smeared-out hyperfine pattern attributed to the averaging of the hyperfine interactions due to through-space and/or through-bond intramolecular exchange couplings.

The isolated molecule has also been studied in a polystyrene matrix (ca. 3% w/w). The main signal is a unique band centered at $g = 2.007$, and additional weak lines are observable on both sides (Figure 3a). The intense central peak cannot be attributed to a doublet species, as are the frequently observed single radical impurities in biradicals. It must be attributed to strong exchange narrowing effects of the dipolar interaction, resulting in the observed fine structure pattern. As a matter of fact, the temperature dependence of the $\Delta M_S = \pm 1$ central line is well fitted by a singlet−triplet equilibrium with a singlet ground state and a singlet−triplet splitting (Figure 3b) in good agreement with the estimation from the SQUID measurements: $\Delta E_{ST} = 479 \pm 3$ K ($R = 0.9995$). This observation confirms the absence of intermolecular interactions in the crystalline material. The small signals of Figure 3a correspond to a triplet species with a zero field splitting (ZFS), $D' = D/g\mu_B$, parameter of 168 G, in agreement with the reported value measured in 2-methyl-

(35) Bleaney, B.; Bowers, K. D. *Proc. R. Soc. London, Ser. A* **1952**, *214*, 451.
(36) (a) Wertz, J. E.; Bolton, J. R. *Electron Spin Resonance: Elementary Theory and Practical Applications*; Chapman and Hall: New York-London; 1986; pp 250 ff. (b) Catala, L.; Turek, P. *J. Chim. Phys.* **1999**, *96*, 1551.

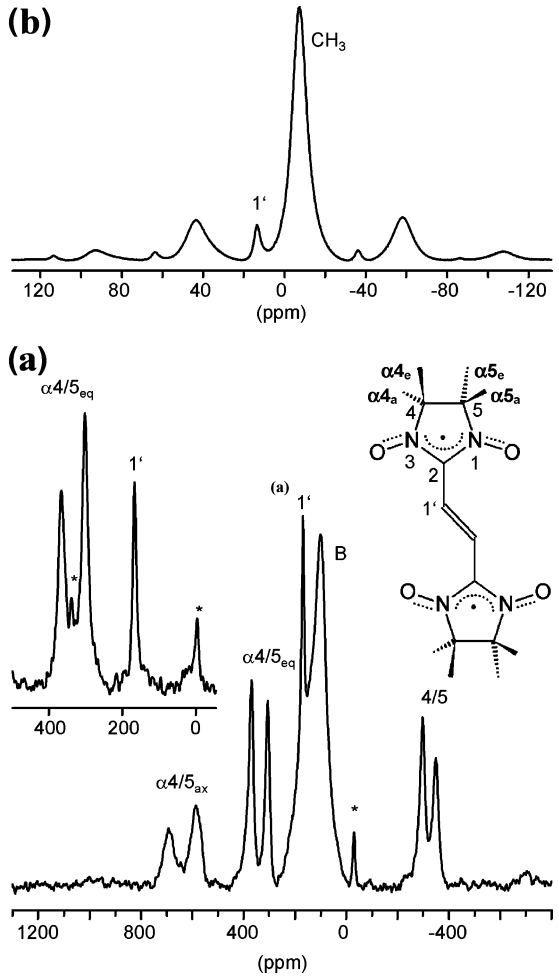

Figure 4. (a) ^{13}C MAS NMR spectrum of **D-NIT2** (T = 307 K, spinning rate 14.5 kHz, B = background signal, * = spinning sidebands); inset: selected range of the spectrum recorded with background suppression. (b) ^{1}H MAS NMR spectrum obtained under the same conditions.

tetrahydrofuran glass (D' = 170 G).[34] Within the point-dipole approximation,[37] D' yields an interspin distance of 5.49 Å, which is much larger than the distance of about 3.8 Å between the two α−C atoms of the five-member rings. This discrepancy cannot be ascribed to conformational changes, which would hardly affect the interspin distance. Rather, it points to the breakdown of the point-dipole approximation owing to the observed strong exchange interaction and spin delocalization (see NMR part below), which are not included in the approach. The anisotropy component, E′, of the dipolar field could not be assessed, because the *y*-components of the triplet pattern are hidden under the central signal. A half-field signal corresponding to $\Delta m_S = \pm 2$ was detected below 128 K. Its intensity decreased rapidly with decreasing temperature so that the temperature dependence could not be studied properly.

Solid-State NMR Spectroscopy. From polycrystalline samples of **D-NIT2** ^{13}C and ^{1}H NMR, spectra have been obtained under magic angle spinning (MAS) conditions. A representative example is given in Figure 4a. Each of the magnetically nonequivalent carbon atoms shows a separate signal except for C2. We ascribe the failure to detect C2 to fast nuclear spin relaxation, caused by the large spin density on C2, and to a large shift anisotropy, which spreads the spinning sideband pattern beyond the detection limit of the individual components. Qualitatively, the main NMR features correspond to what has been found previously for nitronyl-nitroxides.[38] For instance, the signals of C4/5 appear at low frequency. Based on the fact that the NMR signal shift is proportional to the amount and the sign of the unpaired electron spin density at the observed nucleus, the spin density at C4/5 is negative. Correspondingly, positive spin density is found at the methyl carbon atoms. As the imidazoline five rings of the nitronyl-nitroxides are puckered, two of the four methyl groups are oriented parallel (equatorial), and two perpendicular (axial) with respect to the five rings. The latter have more strongly shifted ^{13}C NMR signals because the hyperconjugational spin transfer from the NO groups (the actual spin sources) is more efficient due to better overlap between the spin-containing p-orbitals at the nitrogen and the C−C bond involving the methyl group. Note that the low crystal symmetry implies nonequivalent equatorial and axial methyl groups, respectively. The remaining signal near 170 ppm belongs to the olefinic bridge between the two nitronyl-nitroxides. It is somewhat disturbed by a background signal of the probe head. Suppression of the background signal by an appropriate pulse sequence (inset in Figure 4a) shows that there is no other signal in this spectral region and that the compound is pure.

Table 1. ^{13}C and ^{1}H MAS NMR Contact Shifts[a] (δ^{con}) and Spin Densities[b] (ρ) of the Bridged Nitronyl-Nitroxide **D-NIT2**

nucleus and position[c]	D-NIT2	
	δ^{con}	ρ
C$\alpha 4_{ax}$[d]	671	5.82
C$\alpha 5_{ax}$[d]	564	4.89
C$\alpha 4_{eq}$[d]	346	3.00
C$\alpha 5_{eq}$[d]	284	2.46
C4[d]	−416	−3.61
C5[d]	−365	−3.16
C1′	12	0.10
Hα1′	6.2	0.05
Hβ4/5	−8.5	−0.07

[a] In ppm at 307 K. [b] In au × 10^{-3}. [c] For numbering, see Figure 4. [d] Interchange of the respective signals not excluded.

In the ^{1}H MAS NMR spectrum of **D-NIT2** (Figure 4b), the methyl signals appear near −7 ppm. Unlike the ^{13}C MAS NMR spectrum, they are not resolved because the signal half width (2700 Hz) is larger than the shift difference. Furthermore, the olefinic protons give rise to one well-resolved signal at about 13 ppm. The data of **D-NIT2** are collected in Table 1. All data are contact shifts, δ^{con}, which were obtained after correcting the experimental signal shifts for the diamagnetic contribution (see Experimental Section). The dipolar shift was neglected because, according to the EPR spectra, the *g*-factor anisotropy was immeasurably small. The δ^{con} values were converted to the spin densities at 307 K as described previously[38] by using g = 2.0067 obtained from the EPR spectra.

A striking feature of the NMR data of **D-NIT2** is that all NMR signals are considerably less shifted than those known for nonbridged nitronyl-nitroxides.[39] For instance, the axial methyl carbon signals of **D-NIT2** appear near 600 ppm (rather than near 1100 ppm), and corresponding differences exist for the equatorial methyl carbon signals (about 300 ppm versus 450 ppm) and the methyl proton signals (about −7 ppm versus −14

(37) Rassat, A. *Pure Appl. Chem.* **1971**, *25*, 623.

(38) Heise, H.; Köhler, F. H.; Mota, F.; Novoa, J. J.; Veciana, J. *J. Am. Chem. Soc.* **1999**, *121*, 9659.

(39) Köhler, F. H. In ref 1d; Vol. 1, p 379.

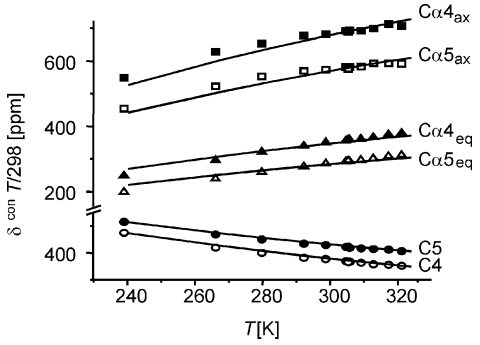

Figure 5. Plot of the reduced contact shifts of **D-NIT2** versus temperature.

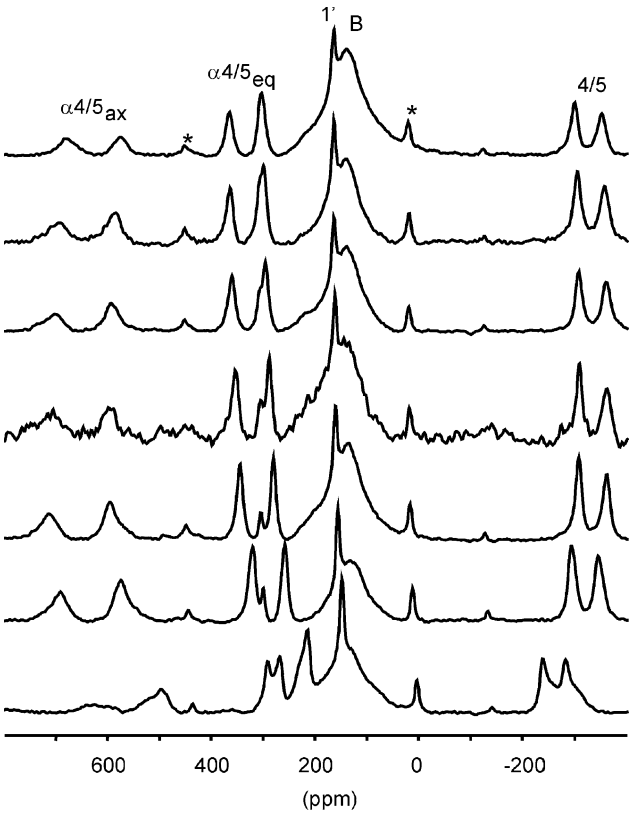

Figure 6. Temperature-dependent ^{13}C MAS NMR spectra of **D-NIT2** (spinning rate 12 kHz, B = background signal, * = spinning sidebands, temperatures from top to bottom: 324, 320, 316, 312, 307, 301, 295, 282, 268, 240 K).

ppm). The decrease of the signal shifts is a signature of the intramolecular antiferromagnetic interaction between the nitronyl-nitroxide moieties, which reduces the time average of the spin density throughout the molecule as the total electron spin singlet state is favored over the triplet state.

Another consequence of the antiferromagnetic coupling is the temperature dependence of the contact shifts. If the Curie law is obeyed (i.e., in the absence of interactions between the electron spins), the reduced contact shifts $\vartheta^{con} = \delta^{con} \cdot T/298$ K are independent of the temperature. It can be seen in Figures 5 and 6 that this does not apply for **D-NIT2**. Rather, the magnitudes of all reduced contact shifts vary with T like the magnetic susceptibility (Figure 2). As has been shown for antiferromagnetically coupled organometallic compounds,[40] the

(40) (a) Hilbig, H.; Hudeczek, P.; Köhler, F. H.; Xie, X.; Bergerat, P.; Kahn, O. *Inorg. Chem.* **1998**, *37*, 4246. (b) Hilbig, H.; Köhler, F. H. *New J. Chem.* **2001**, *25*, 1152.

Table 2. Magnetic Interaction Constants (J) and Limiting NMR Contact Shifts (ϑ^{con}_{∞}) of **D-NIT2** Obtained from Fits of the Temperature-Dependent NMR Data

fitted signals	J [K]	ϑ^{con}_{∞} [ppm]
$C\alpha4_{ax}$[a]	−433	1226
$C\alpha5_{ax}$[a]	−420	1029
$C\alpha4_{eq}$[a]	−570	831
$C\alpha5_{eq}$[a]	−594	732
C4[a]	−505	−771
C5[a]	−502	−870

[a] Interchange of the respective signals not excluded.

Scheme 2. Signs of the Spin Density on Selected Carbon Atoms of **D-NIT2** (see text for details)

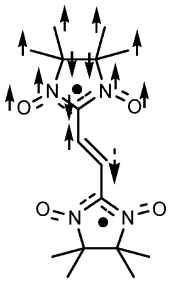

NMR data can be fitted to an equation,[41] which is derived from the Dirac−Heisenberg−Van Vleck model and which, in the case of **D-NIT2**, is given by

$$\vartheta^{con} = \frac{2A}{3\gamma h} \frac{g_e^2 \beta_e^2}{k298} \frac{1}{3 + \exp(-J/kT)} \qquad (1)$$

In eq 1, γ is the gyromagnetic ratio, g_e, the electron g-factor, β_e, the Bohr magneton, and k, the Boltzmann constant. The fit yields the magnetic interaction constant J and the hyperfine coupling constant A of the nucleus of interest. A can be converted to a limiting contact shift, ϑ^{con}_{∞}, that the nucleus would have at infinite temperature, i.e., if the two nitronyl-nitroxide moieties were magnetically independent. The fitting results in Table 2 show some scatter of J, but the mean value of $J = -504$ K is in reasonable agreement with that obtained from the fit of the magnetic susceptibility ($J = -460$ K) and the EPR data ($J = -479$ K). Also, the limiting contact shifts lie well in the ranges known from other nitronyl-nitroxides.[38,39] The scatter of J is probably due to some dynamic behavior which modulates the temperature-dependent NMR data. Actually, it has been concluded from ^{13}C MAS NMR spectroscopy that nitronyl-nitroxides vibrate in the lattice.

The experimental spin density patterns of the carbon skeletons of **D-NIT2** is visualized in Scheme 2 where arrows pointing up represent a positive sign and vice versa. When starting from the NO spin sources of the upper nitronyl-nitroxide moiety, the sign of the spin density changes on passing from one carbon atom to the next until the middle of the bridge is reached. If we continue down the molecule, the broken arrows are expected, which are opposite to the observed spin signs, and the same is true if we extend the arrow pattern into the second nitronyl-nitroxide moiety. The reason is that for those atoms the spin density transferred from the lower nitroxide radical prevails. The transfer of spin density of opposite sign from both radical moieties leads to a partial cancellation of spin density which

(41) Banci, L.; Bertini, I.; Lucinat, C. *Struct. Bonding* **1990**, *72*, 113.

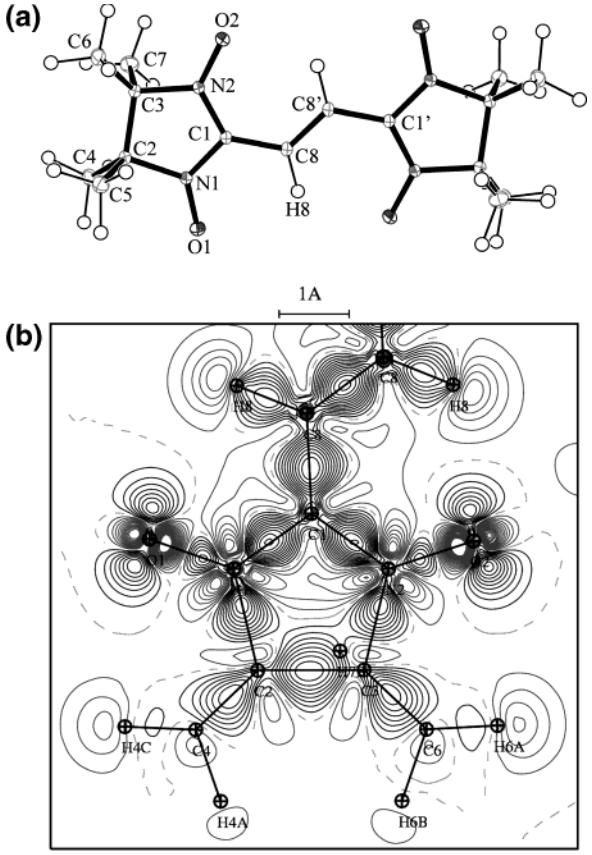

Figure 7. (a) ORTEP view of the **D-NIT2** radical at 110 K. Thermal ellipsoids are plotted at the 50% probability level. (b) Static deformation density in the mean plane of the **D-NIT2** molecule. Contours of 0.05 eÅ^{-3} (positive contours in red lines, negative contours in blue lines, and long dashed green lines for zero contour).

Table 3. Topological Properties of ρ at the Bond Critical Points (CP) and Net Charges Obtained by Electronic Density Integration over Atomic Basins

A	B	A–CP distance (Å)	CP–B distance (Å)	$\nabla^2\rho_{(r)}$ (eÅ^{-5})	ρ (eÅ^{-3})	ϵ	λ_3
N_1	O_1	0.640	0.635	−2.48	2.72	0.23	39.5
N_2	O_2	0.645	0.632	−3.40	2.67	0.14	37.7
C_1	N_1	0.540	0.825	−19.40	2.13	0.39	11.2
C_1	N_2	0.532	0.822	−21.78	2.21	0.35	11.2
C_2	N_1	0.623	0.884	−8.38	1.59	0.10	11.4
C_3	N_2	0.614	0.891	−7.71	1.57	0.10	11.4
C_3	C_2	0.773	0.791	−9.01	1.55	0.02	9.54
C_4	C_2	0.709	0.815	−10.63	1.61	0.04	8.84
C_5	C_2	0.716	0.816	−10.35	1.58	0.03	8.88
C_6	C_3	0.728	0.795	−11.11	1.66	0.08	9.11
C_7	C_3	0.735	0.797	−10.51	1.66	0.06	9.41
C_8	C_1	0.677	0.759	−16.04	1.85	0.18	7.94
C_8	C_8	0.681	0.681	−21.73	2.12	0.36	6.68
H_{6B}	O_2	0.871	1.383	1.45	0.06	0.02	1.95
H_8	O_2	0.943	1.352	1.53	0.09	0.12	2.24

atom	net charge (e)	volume (Å^3)
O1	−0.33	19.21
O2	−0.29	19.45
N1	−0.64	9.51
N2	−0.60	11.21
C1	0.60	10.24
C2	−0.12	6.41
C3	−0.10	6.40
C4	0.05	10.55
C5	0.15	9.54
C6	0.08	9.88
C7	0.10	9.31
C8	0.17	14.33
H_{me}	0.07	5.99
H8	0.17	6.69

explains the strikingly small paramagnetic signal shifts of both carbon and hydrogen atoms of the olefinic bridge in **D-NIT2**.

To better explore the possible mechanisms governing this very efficient magnetic interaction, we have undertaken a detailed analysis of the electron density distribution obtained from accurate single-crystal X-ray diffraction measurements.

Electron Density. An ORTEP[42] view of the asymmetric unit and the static deformation density in the **D-NIT2** molecular plane are shown in Figure 7a and b, respectively. The static deformation density maps reveal the electron density change due to the bonding interactions by reference to the independent atom model of electron density (IAM); they are similar to those obtained for two related NN radicals,[38,39] with a low deformation density in the N−O bond, a negative density at the N and O nuclei, and lone pairs perpendicular to the N−O bond. These features are the clear electronic signature of the N−O radical; some differences in the NO charge density show up at the oxygen lone pairs sites: their static density is more concentrated than those observed in previous studies. This is due to the different packing of the three compounds (HC≡CpyNIT,[32] NITPhSMe,[31] and **D-NIT2**). In NITPhSMe and HC≡CpyNIT, many hydrogen bonds involve the NO radical and then contribute to a charge and spin transfer from the lone pairs density to the neighboring molecules, while **D-NIT2** exhibits only one long intermolecular contact (O2···H6B = 2.24 Å).

Compared to NITPhSMe, **D-NIT2** is an almost perfectly conjugated system with a dihedral angle between radicals of less than 2°. These geometric characteristics can be quantified by the topological analysis of the O—N—C—N—O electron density (Table 3): whereas the positions of the critical points (CP) and their density are very close to those observed for NITPhSMe, the Laplacians, the charge, and the ellipcity of the N—O bonds are however different. The lack of intermolecular interactions is revealed by the oxygen and nitrogen topological charges and volumes of the O—N—C—N—O group which are larger in **D-NIT2**: −1.25 e and 69.6 A^3 compared to −0.92 e and 59.00 A^3 for NITPhSMe. The conjugation effect in **D-NIT2** is very well pictured by the deformation maps perpendicular to the N1—C1, C1—C8, and C8—C8 bonds (Figure 8). This is in line with the ellipticities observed (Table 3), which show a large $\sigma-\pi$ character of the O—N—C1—C8═C8′ bonds allowing a strong electronic delocalization through the C1—C8—C8b—C1b bridge between the two connected NN functions.

The topological analysis also reveals the two hydrogen bonds existing in the crystal, the first being intramolecular, between O2 and H8A, $A = (-x, 2 - y, -z)$, (H8A···O2 = 2.25 Å; ρ_{CP} = 0.09 eÅ^{-3}), and the second being an intermolecular one, which relates O2 and H6B, $B = (-x, {}^1/_2 + y, {}^1/_2 - z)$ (H6B···O2 = 2.24 Å, ρ_{CP} = 0.06 eÅ^{-3}). The critical point of the first interaction leads to the formation of a cycle associated with a ring critical point involving O2, N2, C1, C8A, H8A. Between room temperature and 106 K, the intramolecular

(42) Johnson, C. K. ORTEP II. Report ORNL-5738. Oak Ridge National Laboratory, Tennessee, USA, 1976.

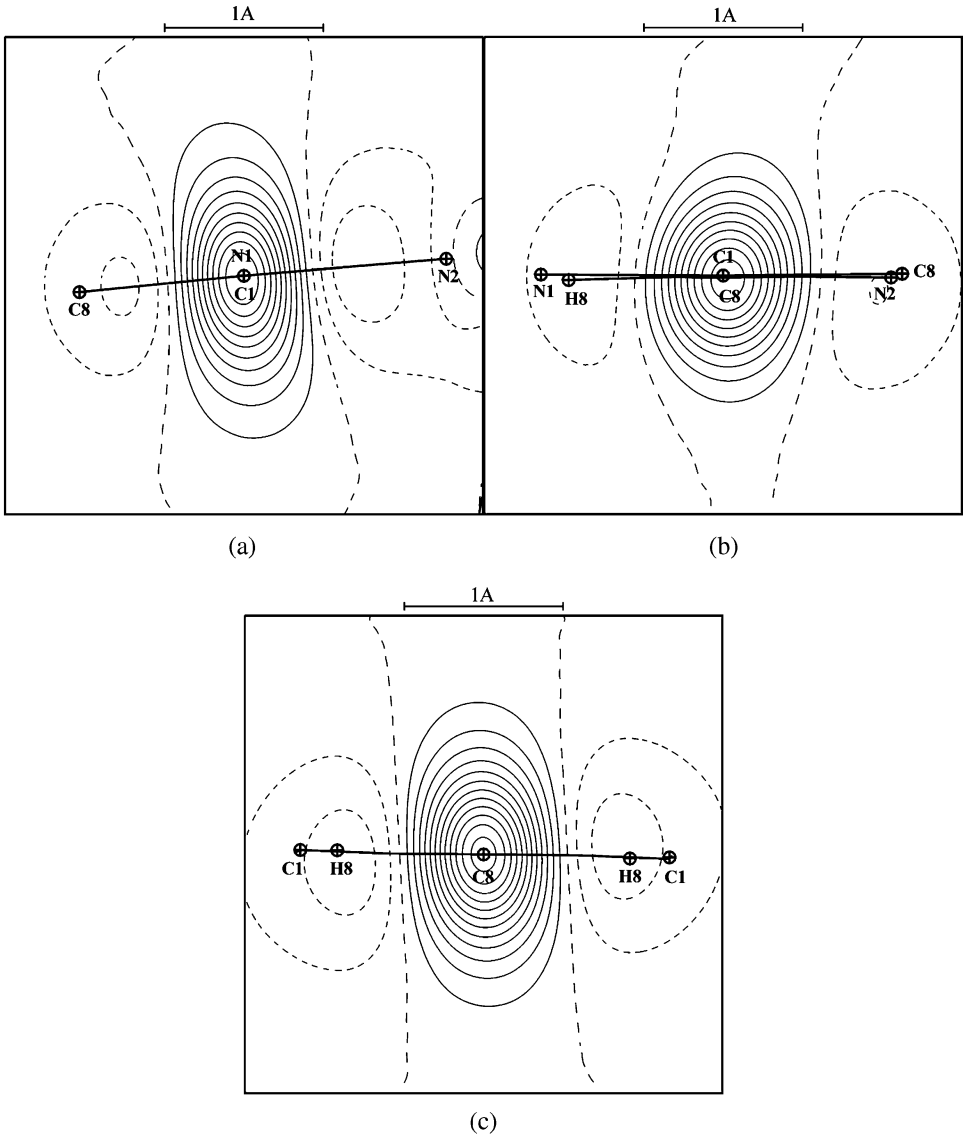

Figure 8. Static deformation density maps in planes perpendicular to the N1−C1 (a), C1−C8 (b), and C8−C8 (c) bonds. Contours of 0.05 eÅ^{-3}: positive contours in solid lines, negative contours in short dashed lines, and long dashed line for zero contour.

distance O2···C8A increased from 2.864 to 2.941 Å (2.7%), whereas O2···H8A decreased from 2.587 to 2.255 Å (12.8%). This leads to a more compact ring and results in a significant accumulation of electron density at this ring critical point. At the unit cell level, the cell parameters decrease from room temperature to 106 K by 1.81, 0.30, and 0.49% for **a**, **b**, and **c**, respectively, and the only notable intermolecular contact revealed by the topological analysis, O2···H6b, is roughly oriented along the **b** direction; this contact should then not be significantly affected by the thermal contraction. On the other hand, between room temperature and 106 K, the distance O2···C6B decreased from 3.69 to 3.29 Å (10.8%), and O2···H6B, from 2.89 to 2.24 Å (19.0%), whereas the distance C3···C6B was not modified. This implies a major reorientation of the molecules, thereby reducing intermolecular space.

Conclusion

The detailed analysis of the magnetic and electronic properties of a conjugated biradical revealed that a double bond is highly suitable for promoting very strong antiferromagnetic exchange interactions between the radical centers. Despite the fact that a geometrical approach for determining the sign of exchange interactions does not show any systematic correlation, the antiferromagnetic interaction found in the present molecules is in keeping with the McConnell[43] and Kahn/Briat[44] models. Solid-state ^{1}H and ^{13}C MAS NMR spectroscopy confirmed the geometry of the biradicals as determined by single-crystal X-ray analyses and proved the absence of any diamagnetic impurities. Conversion of the NMR signal shifts into spin densities afforded an almost complete spin map, while the temperature dependence of the contact shifts confirmed the large antiferromagnetic exchange interaction constant determined by magnetic susceptibility and EPR measurements. The study of the topological properties of all bonds revealed the electron delocalization from one radical to the other through the double bonds. The fact that a double bond is a particularly good radical linker was reflected by electron density studies. Further studies are now directed toward the preparation of paramagnetic molecules where the spin polarization should favor intramolecular ferromagnetic pathways.

(43) McConnell, H. M. *J. Chem. Phys.* **1963**, *39*, 1910.
(44) Kahn, O.; Briat, B. *J. Chem. Soc., Faraday Trans 2* **1976**, *72*, 268.

Experimental Section

Synthesis. D-NIT2. *N*,*N*′-Dihydroxy-2,3-diammonium-2,3-dimethylbutane sulfate (300 mg, 1.22 mmol) is dissolved in water (5 mL). (1*E*)-1,2-Bisdimethylacetal-ethene (97 mg, 0.55 mmol) in methanol (1 mL) is added, and the mixture is heated (60 °C). After 3.7 h, the brown solution is cooled to 20 °C and is neutralized with an aqueous solution of $NaHCO_3$. The mixture is evaporated to dryness, and CH_2Cl_2 is added (100 mL). $NaIO_4$ (720 mL, 3.37 mmol) in water (100 mL) is added, and the biphasic mixture is stirred during 50 min. After separation of the organic layer and extraction with CH_2Cl_2 (100 mL), the solvents are evaporated. The pure product is obtained after chromatography (SiO_2 flash, elution: CH_2Cl_2 to CH_2Cl_2−0.5% MeOH) and recrystallization from CH_2Cl_2/hexane. Yield: 49 mg, 26%. EI^+ *m*/*z* (relative intensity in %): 338.2 $[M]^+$ (100), 322.1 $[M-O]^+$ (30), 306.1 $[M-2O]^+$ (20), 290.1 $[M-3O]^+$ (<5). IR (KBr, cm^{-1}) 1427, 1376 (ν_{NO}), 1259, 1208, 1137, 1107, 990, 868, 619, 544. UV−vis (CH_2Cl_2) λ (nm) (ϵ, M^{-1} cm^{-1}) 575 (390), 401 (13 620), 354 (36 775), 269 (11 110), 236 (15 910). Elemental analysis calculated for $C_{16}H_{26}N_4O_4$ (M = 338.41): C, 56.79; H, 7.74; N, 16.56. Found: C, 56.60; H, 7.55; N, 16.37.

X-ray Crystal Structure Analysis. The intensity data were collected in the phi scan mode at 294 K for **D-NIT2** on a Kappa-CCD diffractometer equipped with a graphite monochromator for the Mo Kα radiation. Cell constants were derived from a least-squares fit of the setting angles for 25 selected reflections with $10° < q < 15°$. The intensities were corrected for Lorentz and polarization effects but not for absorption. The atoms were located in a succession of difference Fourier syntheses and were refined with anisotropic thermal parameters using the SHELX76 and SHELX85 packages.[45] The hydrogen atoms were included in the final refinement model in calculated and fixed positions with isotropic thermal parameters. Crystal structure and refinement data are summarized in Table S1.

Charge Density Modelisation. A. Data Collection. A **D-NIT2** single crystal of 0.65 × 0.51 × 0.60 mm^3 was mounted on a Nonius Kappa-CCD diffractometer using graphite monochromatized Mo Kα radiation (λ = 0.710 73 Å); the relatively large size of the sample is justified by the low diffracting power of the crystal. The crystal was cooled to 106 K using an N_2 Oxford cryosystem cooling device. The final cell parameters (a = 6.0758(1), b = 11.0612(2), c = 13.0663(2) Å, β = 99.179(1)), were obtained at the end of the overall data collection by refinement against all the collected reflections. Reflections were integrated using the program DENZO[46] implemented in the HKL2000[46] package. Then, the data were corrected from absorption effects using ABSORB[47] program and finally sorted, scaled, and averaged using SORTAV.[47] The crystal did not present any decay during the data collection as checked by the evolution of the interframe scale factors versus time. The 112 757 observed reflections were merged into 15 010 independent reflections with an overall completeness of 97.1%, leading to a good redundancy (7.5 on average), necessary for an accurate charge density study. The internal agreement index for the whole data set is R_1 = 3.48% without any σ cutoff. Crystal structure and refinement data are summarized in Table S2.

B. Charge Density Refinements. First, the crystal structure was solved using the SHELX package[48] and refined against X-ray diffraction data at 106 K ($R_1(F^2)$ = 3.4%, for 8505 reflections with $I > 2\sigma$ and 161 parameters). To model accurately the electron density distribution, a Hansen−Coppens refinement was performed (Program MOPRO [49]):

$$\rho(\vec{r}) = \rho_{core}(r) + P_v\kappa^3\rho_v(\kappa r) + \sum_{l=0}^{l_{max}}\kappa'^3 R_l(\kappa' r)\sum_{m=0}^{+1}\sum_{p} P_{lmp}y_{lmp}(\theta,\varphi) \quad (2)$$

$\rho_{core}(r)$ and $\rho_v(r)$ represent the core and valence densities spherically averaged, calculated from Clementi and Raimondi wave functions of free atoms.[50] The last term correspond to the nonspherical deformation due to the chemical bonding expressed as a projection of the density on a spherical harmonics (in real form (y_{lmp})) basis multiplied by a Slater type radial function $R_l(\kappa' r)$. The refined parameters are P_v (valence population), P_{lmp} (the multipole populations), and κ, κ' (contraction expansion parameters).

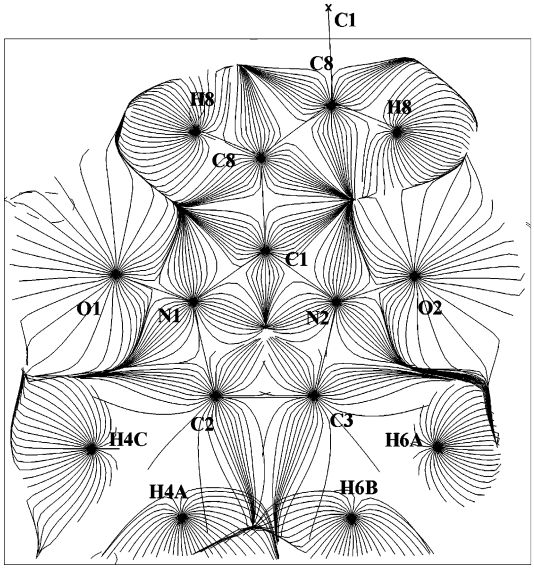

Figure 9. Gradient trajectories in mean plane of the molecule.

The static deformation density is the difference between the modeled static total electron density (eq 2) and the sum of spherical averaged independent atom densities (IAM model):

$$\Delta\rho(\vec{r}) = P_v\kappa^3\rho_v(\kappa r) - N_v\rho_v(r) + \sum_{l=0}^{l_{max}}\kappa'^3 R_l(\kappa' r)\sum_{m=0}^{+1}\sum_{p} P_{lmp}y_{lmp}(\theta,\varphi) \quad (4)$$

where N_v is the number of valence electrons of the free atom. At this final stage of the refinement, R = 3.27%, wR = 2.71%, GOF = 0.63 for 12 042 reflections with $I > \sigma$.

C. Topology of the Electron Density. The total electron density can be analyzed in a more quantitative way using the theory "Atoms In Molecules, A Quantum Theory" developed by Bader.[51] From the spatial distribution of the electron density, one can derive the gradient trajectories $\nabla\vec{\rho}$ (see Figure 9), the Laplacian distribution ($\nabla^2\rho_{(r)}$) (see Figure 10), and the location of all critical points (CP) (i.e., points where the gradient of ρ vanishes) and their associated topological features. The nature of the CP is determined by the eigenvalues (curvatures) of the Hessian matrix:

$$\frac{\partial^2\rho(r)}{\partial x_i\,\partial x_j}$$

The topological analysis of the total electron density allows also the partitioning of space into atomic basins, and the integration of the density over these basins gives access to the net atomic charges. A new version of the program NEWPROP[52] was used to locate the CP

(45) (a) Sheldrick, G. M. *Crystallographic Computing 3*; Sheldrick, G. M., Kruger, C., Goddard, R., Eds.; Oxford University Press: Oxford, U.K., 1985; p 175. (b) Sheldrick, G. *System of Computing Programs*; University of Cambridge: U.K., 1976.
(46) Otwinowski, Z.; Minor, W. *Methods in Enzymology*, 276, *Macromolecular Crystallography*, part A., 307; Carter, C. W., Jr., Sweet, R. M., Eds.; Academic Press: New York, 1996.
(47) DeTitta, G. T. *J. Appl. Crystallogr.* **1985**, *18*, 75.
(48) Blessing, R. H. *J. Appl. Crystallogr.* **1989**, *22*, 396.
(49) Hansen, N. K., Coppens, P. *Acta Crystallogr.* **1978**, *A34*, 909.
(50) Clementi, E.; Raimondi, D. L. *J. Chem. Phys.* **1963**, *41*, 2686.
(51) Bader, R. F. W. *Atoms in Molecules: a Quantum Theory*. The International Series Monographs in Chemistry; Oxford Clarendon Press: 1990.
(52) Souhassou, M.; Blessing, R. H. *J. Appl. Crystallogr.* **1999**, *32*, 210.

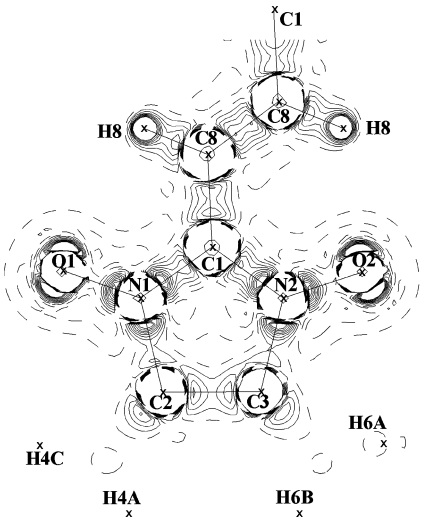

Figure 10. Laplacian of the total electron density in the nitronyle-nitroxyde ring. Contours of 5 eÅ^{-3}: negatives isovalues in solid red lines, zero contour and positives isovalues in dashed blue lines.

and to calculate the topological properties of the modeled electron density and to determine the net atomic charges.

Magnetic Susceptibility Measurements. The magnetic susceptibility was measured on the bulk polycrystalline material in the 2−300 K temperature range for each compound with a Quantum Design MPMS superconducting SQUID magnetometer operating at a field strength of 0.5 T or with an M 8100 SQUID susceptometer from Métronique operating at a field strength of 0.1 T. The data were corrected for the magnetization of the sample holder contribution, and the magnetic susceptibilities were corrected for the diamagnetism of the molecules by fitting the high-temperature data of the χT versus T curve or by estimating its contribution from Pascal's table.

SQUID susceptibility fitting has been performed according to the expression:

$$\chi = \chi_{ST} + \chi_{imp}$$

$$\chi_{ST} = \frac{C}{T} \times \frac{3}{3 + \exp(-J/kT)}; C = \frac{2Ng^2\mu_B^2}{3k}$$

$$\chi_{imp} = \frac{C_{imp}}{T}$$

The software for data fitting is KaleidaGraph (version 3.6, June 26, 2003) supplied by Synergy Software. The impurity content (in χ_{imp}) is estimated with respect to the Curie constant of 0.375 emu K mol^{-1} expected for one spin $S = {}^1/_2$ per molecule. The found value for χ_{imp} is $\chi_{imp} = (0.000\ 204\ 79 \pm 0.000\ 005\ 00)$ emu K mol^{-1}.

EPR Measurements. The EPR measurements were performed with an X-band (microwave frequency: ca. 9.8 GHz) spectrometer (Bruker ESP 300E) equipped with a rectangular TE 102 cavity. The available temperature range was 4−300 K with a continuous flow cryostat (Oxford ESR 900) operating with liquid helium. The temperature (±1 °C) was determined with a Au−Fe/Chromel thermocouple located within the sample tube close to the sample. All samples (1.2×10^{-5} M) were deoxygenated by vigorous Ar bubbling through the solution prior to EPR studies. We have checked by dilution experiments that under this concentration no aggregation favoring intermolecular Heisenberg exchange effects is effective. Care has also been taken in order to avoid microwave saturation phenomena or overmodulation effects on the EPR signal.

^{13}C and ^{1}H MAS NMR Spectra. The ^{13}C and ^{1}H MAS NMR spectra were recorded with Bruker MSL 300, Avance 300, and Avance 400 spectrometers. Microcrystalline samples of **D-NIT2** were mixed in a glovebox with 8% of nickelocene, which was used as internal temperature standard.[53] Subsequently, the powder was packed into ZrO_2 rotors with a 4 mm diameter and sealed with Kel-F caps. The free induction decays were sampled after applying single pulses of 4 μs duration and 5 Hz repetition rate. For the elimination of the probe head signal, the DEPTH pulse sequence[54] was used. Data handling included reverse linear prediction, exponential multiplication up to the magic filter, and baseline correction. The experimental signal shifts, δ^{exptl}, were determined relative to external adamantane ($\delta(^{13}CH_2) = 29.5$, $\delta(^1H) = 2.0$). The contact shifts were obtained after subtracting from δ^{exp} the signal shifts of corresponding nuclei of diamagnetic reference compounds. Since diamagnetic analogues of **D-NIT2** are not available, the signal shifts of a documented 3-(1,3-dihydroxy-4,4,5,5-tetramethylimidazoline-2-yl)pyridine were used: ($\delta(CH_3) = 1.07$, $\delta(CH_3) = 20.7$, δ(C4/5) = 66.3).[37]

Other Instrumentation. UV−vis spectra: Unikon 933 (Kontron Instruments) spectrophotometer. FT-IR spectra: Bruker IFS 25 spectrometer; KBr pellets. Fast-atom bombardment (FAB, positive mode) ZAB-HF-VG-Analytical apparatus with *m*-nitrobenzyl alcohol (*m*-NBA) matrix.

Acknowledgment. We are indebted to Dr. H. Förster, Bruker Biospin GmbH, for recording the low-temperature NMR spectra. Financial support was provided by CNRS and le Ministère de la Recherche et des Nouvelles Technologies.

Supporting Information Available: EPR spectrum of **D-NIT2** in fluid solution at rt (Figure S1) and crystal structure and refinement data are summarized for the X-ray structure determined at 298 K (Table S1) and 106 K (Table S2). This material is available free of charge via the Internet at http://pubs.acs.org.

JA0305959

(53) Heise, H.; Köhler, F. H.; Xie, X. *J. Magn. Reson.* **2001**, *150*, 198.
(54) Cory, D. C.; Ritchey, W. M. *J. Magn. Reson.* **1988**, *80*, 128.